metals

MDPI

Article

Ageing of Al-Mn-Cu-Be Alloys for Stimulating Precipitation of Icosahedral Quasicrystals

Tonica Bončina [1,*], Mihaela Albu [2] and Franc Zupanič [1]

[1] Faculty of Mechanical Engineering, University of Maribor, SI-2000 Maribor, Slovenia; franc.zupanic@um.si
[2] Graz Centre for Electron Microscopy, A-8010 Graz, Austria; mihaela.albu@felmi-zfe.at
* Correspondence: tonica.boncina@um.si; Tel.: +386-2-220-7863

Received: 27 May 2020; Accepted: 9 July 2020; Published: 11 July 2020

Abstract: In this work, the ageing of some Al-Mn-Cu-Be alloys was investigated in the temperature range in which predominantly icosahedral quasicrystalline (IQC) precipitates can form. The alloys were cast into a copper mould, directly aged (T5 heat treatment) between 300 and 440 °C for different times. Afterwards, they were examined using scanning and transmission electron microscopy, X-ray diffraction and hardness testing. The main aim of the work was to determine the conditions at which a high number density of spherical icosahedral quasicrystalline precipitates can form. The highest number density of IQC precipitates was obtained at 300 °C after prolonged ageing. The spheroidal precipitates had a diameter less than 20 nm. The size of IQC precipitates increased with the increasing temperature, and in addition, decagonal quasicrystalline precipitates appeared. The time to maximum hardness decreased strongly with increasing ageing temperature. The IQC precipitates can form in a fairly broad temperature range in Al-Mn-Cu-Be alloys and that by varying ageing temperature and duration, rather different distributions of precipitates can be obtained. The presence of precipitates caused rather strong aluminium alloys and fast work hardening during initial plastic deformation.

Keywords: aluminium; ageing; quasicrystal; transmission electron microscopy

1. Introduction

Quasicrystals were discovered in Al-Mn alloys [1]. Since an icosahedral quasicrystalline phase (IQC) in these and similar alloys is metastable [2], the alloys have been predominantly fabricated by rapid solidification and then, compacted [3]. Rapid solidification enables the formation of very small particles, which can slightly coarsen during compaction, but a fine distribution of quasicrystalline particles can provide high strength [4]. The alloying of Al-Mn alloys with Be, Ce, Si or Fe can stimulate the formation of IQC particles during solidification with slower cooling rates [5–8], however, their sizes are coarser, which decreases their strength and toughness.

A fine distribution of particles can be obtained by precipitation hardening, which is a typical hardening process in many aluminium alloys [9–12]. There are several types of precipitates, which are mainly metastable. According to the best of the authors' knowledge, there are no commercial alloys that would be mainly strengthened by icosahedral quasicrystalline particles. The manufacturing of alloys with a high density of IQC precipitates may be a challenge and they can also have an interesting combination of properties. The formation of IQC precipitates was observed in many Al-alloys. Hansen and Gjonnes [13] found that the IQC phase formed during heat treatment of a high-Mn aluminium alloy, and then, transformed to the cubic α-AlMnSi phase. Li and Arnberg [14] studied dispersoids in a commercial 3003 alloy. Some icosahedral quasicrystal dispersoids were found to precipitate at the early stage of precipitation. Mochugovskiy et al. [15] discovered IQC precipitates in an Al-3%Mg-1%Mn alloy during annealing at 360 °C. Partly coherent IQC precipitates predominantly formed on the dislocations and dislocation walls, and were relatively rare.

The IQC precipitates were discovered also in an $Al_{94}Mn_2Be_2Cu_2$ alloy during in situ study of the temperature stability of the IQC phase formed during solidification [16]. During further research, they were found in samples heat-treated at 300 and 400 °C [17]. They did not form at 200 °C because of the very low diffusivity of Mn. Instead, some precipitation of Θ'-Al_2Cu was observed. The T-$Al_{20}Mn_3Cu_2$ precipitates formed at 500 °C, which are also known from other alloys containing Cu and Mn [18]. The IQC precipitates in this alloy have primitive icosahedral structure (space group $Pm\overline{3}5$). They form at least a semi-coherent interface with an aluminium matrix, and possess a specific orientation relationship with it. All aluminium fourfold axes are parallel to three twofold axes of IQC, and at the same time also, threefold aluminium axes are parallel with the threefold axes of IQC [17,19].

Since the precipitation of quasicrystalline precipitates takes place within a temperature range, in which most aluminium alloys rapidly lose their strength, the alloys with quasicrystalline precipitates may be used at high temperature application, e.g., produced by high pressure die-casting or single roll casting, which have moderate cooling rates. One of the main prerequisites is the presence of sufficiently high volume fraction of uniformly distributed IQC precipitates, which has not been achieved in Al-alloys yet.

In our previous work, it was found out that icosahedral quasicrystalline precipitates can form in Al-Mn-Cu-Be alloy during T5 heat treatment at 300 and 400 °C [17]. The IQC precipitate possessed good matching with the Al-rich solid solution α-Al, and have a specific orientation relationship with it [17,19]. It was also discovered that in the alloy Al-Mn-Cu-Be-Sc-Zr, plate-like decagonal quasicrystals formed on the {001} planes of α-Al [19]. These suggested that the Al-Mn-Cu-Be alloys could be used for precipitation hardening. In order to prove this, two Al-Mn-Cu-Be alloys with improved chemical compositions were cast into copper moulds with different diameters to achieve cooling rates 250–600 °C/s and then, aged in the temperature range between 300 and 440 °C for different durations. The primary aim of this investigation was to find the conditions at which a high density of spherical icosahedral precipitates in an Al matrix can be obtained by T5 heat treatment (ageing of samples in the as-cast condition). In addition, the properties of the stronger alloy at room temperature were determined, as well as the microstructures after some degree of plastic deformation.

2. Materials and Methods

The compositions of the investigated alloys are given in Table 1. The manganese content is essential for the formation of quasicrystalline phase during solidification. The addition of beryllium enables formation of the quasicrystalline phase at lower cooling rates and also stimulates formation of quasicrystalline precipitates. By the addition of copper, T-$Al_{20}Mn_3Cu_2$ precipitates can form at higher temperatures, and by application of T6 heat treatment, Cu-rich precipitates can be created. The contents of alloying elements was decreased comparing to the previously studied Al-Mn-Cu-Be alloy, in which IQC precipitates were determined [17].

Table 1. Chemical compositions of the investigated alloys after vacuum induction melting, as determined by Atomic Emission Spectroscopy–Inductively Coupled Plasma (*w*—weight fraction in %, *x*—atomic fraction in %).

Alloy No.	Alloy	*w* (Al)	*w* (Mn)	*w* (Be)	*w* (Cu)	*x* (Al)	*x* (Mn)	*x* (Be)	*x* (Cu)
#1	$Al_{96.5}Mn_{0.8}Cu_{1.2}Be_{1.5}$	Remain	1.55	0.48	2.73	Remain	0.77	1.47	1.18
#2	$Al_{95.4}Mn_{1.8}Cu_{1.6}Be_{1.2}$	Remain	3.51	0.38	3.71	Remain	1.78	1.18	1.63

The alloys were vacuum induction melted using commercially available Al99.8, AlMn10, AlCu25 and AlBe5.5 master alloys into bars with diameters 20 mm, and sectioned to pieces of about 200 g. The pieces were melted and cast into a copper block with a diameter of 110 mm and height of 120 mm, with the casting temperature around 750 °C. The melt solidified in cylindrical holes engraved into the copper block with the diameters of 4, 6 and 10 mm and lengths of 40 mm. The solidification rates before beginning solidification, determined experimentally, were 580 ± 53, 510 ± 44 and 258 ± 31 K s^{-1}

for 4, 6 and 10 mm rod, respectively. After casting, the cast samples were aged artificially in the air at temperatures from 300 to 440 °C for different times. This kind of heat treatment is designated as T5 treatment. During T6 teat treatment, T-$Al_{20}Mn_3Cu_2$ precipitates form on solution annealing, and almost no alloying elements remain available for the formation of quasicrystalline precipitates during ageing.

The basic metallographic analysis was done by Light Microscopy (Epiphot 300, Nikon, Tokyo, Japan) and Scanning Electron Microscopy (Sirion 400 NC, FEI, Eindhoven, The Netherlands) equipped with an Energy Dispersive Spectrometer (INCA x-sight, Oxford Analytical, Bicester, UK). Some samples were investigated after final polishing with a diamond paste (1 μm) only. The samples were etched with a methanol-iodine solution after ageing, which revealed the distribution of precipitates in the microstructure and precipitation free zones [20]. The phase analysis was carried out by XRD (X-ray Diffraction, Sincrotrone Elettra, Trieste, Italy) using synchrotron X-rays with a wavelength of 99.9996 pm. Lamellas for the Transmission Electron Microscopy (TEM) were prepared using a Focused Ion Beam FIB (Helios, FEI, Eindhoven, The Netherlands). High-Resolution TEM (Titan^3 G2 60–300, FEI, Eindhoven, The Netherlands) and Energy-Dispersive X-ray Spectroscopy, EDS (SuperX, Bruker, Billerica, MA, USA) were carried out in an probe corrected electron microscope. The compression test was carried out by a quenching/deformation dilatometer (DIL 805A/D, TA Instruments, New Castle, DE, USA) at room temperature, with the strain rate 0.05 s^{-1}. The sample had 10 mm length and diameter 5 mm. It was machined from the cast bar with a diameter of 6 mm. Two samples were deformed to 0.09 and 0.4 true strain and investigated by TEM. Hardness was measured by a Zwick 3212 with a load of 0.1 kg (HV 1).

3. Results

3.1. As-Cast Condition

In samples with diameters 4 and 6 mm, the columnar α-Al grains with a cellular-dendritic morphology prevailed. Some equiaxed grains were at the centres of the 10 mm in diameter samples. The microstructures of all alloys in the as-cast condition consisted predominantly of three phases, α-Al (Al-rich solid solution), icosahedral quasicrystal (IQC) and Θ-Al_2Cu (Figure 1).

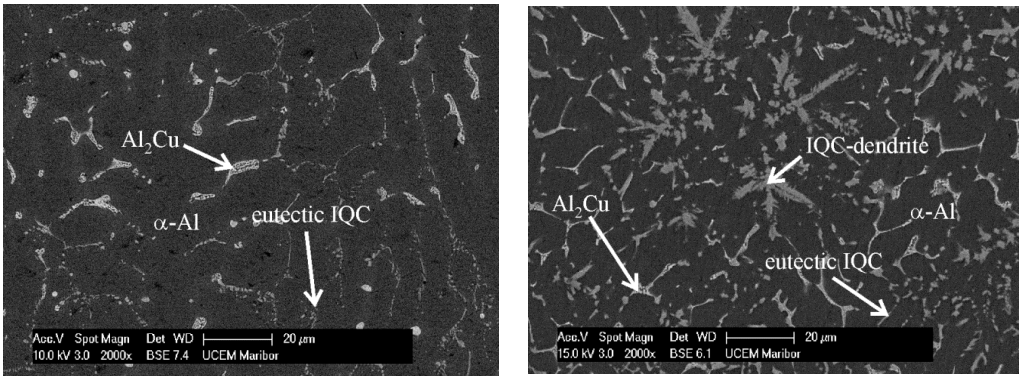

(**a**) (**b**)

Figure 1. Backscattered electron micrographs of the gravitationally cast samples in the as-cast conditions of (**a**) the alloy $Al_{96.5}Mn_{0.8}Cu_{1.2}Be_{1.5}$, (**b**) $Al_{95.4}Mn_{1.8}Cu_{1.6}Be_{1.2}$. Polished samples.

The primary dendritic IQC phase, with dendrite arms extending in the threefold directions, was only present at the centre of the 10 mm sample in the alloy $Al_{95.4}Mn_{1.8}Cu_{1.6}Be_{1.2}$ (Figure 1b). The IQC phase was present as a part of a (α-Al + IQC) binary eutectic (Figure 1). The Θ-Al_2Cu phase was in the interdendritic spaces as a heterogeneous constituent (α-Al + Θ-Al_2Cu). The dendrite arm spacing and the interdendritic areas increased with the specimen size.

The XRD revealed the same phases in the as-cast state as SEM micrographs, α-Al, IQC and Θ-Al_2Cu (Figure 2a). The lattice parameters of the FCC α-Al were similar in all alloys and samples. They were about 403.80 pm, which is 0.28% less than in pure Al (powder diffraction file pdf 000-04-0787). This value indicates that the matrix was supersaturated with Cu and Mn, having the smaller atomic diameters than Al (R_{Al} = 143.2 pm, R_{Mn} = 136.7 pm, R_{Cu} 127.8 = pm). The calculated lattice parameter of *a*(Al) would be 403.82 pm if we apply Vegard's law and assume the maximum equilibrium solubility of Cu and Mn in Al (Mn: 0.62 at. % [21] and Cu: 2.5 at. % [22]). Almost the same values of measured and calculated *a*(Al) strongly suggest a high supersaturation of the matrix. The lattice parameters of Θ-Al_2Cu were nearly the same as in pure Θ-Al_2Cu (pdf 000-89-198), pointing out that it did not dissolve Mn or Be. The IQC phase exhibited wide peaks, arising from small particle sizes and the presence of many defects in them. A strong peak at approximately 27.5° occurred in a 10 mm sample of the alloy $Al_{95.4}Mn_{1.8}Cu_{1.6}Be_{1.2}$, which is designated by (!) in Figure 2a. Its presence testified the existence of an additional phase at the sample centre, belonging probably to $Al_{15}Mn_3Be_2$ [6] or any other metastable phases found in Al-Mn-Cu alloys by Stan-Glowinska [23].

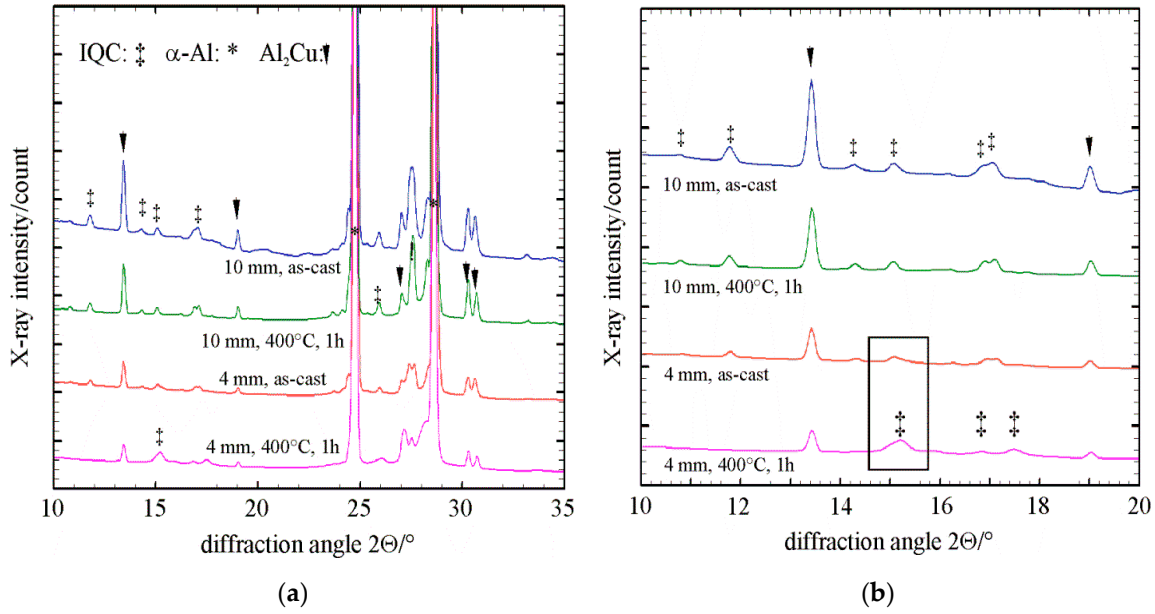

Figure 2. X-ray diffraction patterns of different samples and conditions of the $Al_{95.4}Mn_{1.8}Cu_{1.6}Be_{1.2}$ alloy. (**a**) The range between 10° and 35°, and (**b**) the range between 10° and 20° that shows clearly the positions and shapes of minor phases' peaks.

The highly alloyed $Al_{95.4}Mn_{1.8}Cu_{1.6}Be_{1.2}$ attained the highest hardness in the as-cast state due to the higher phase fraction of IQC and Θ-Al_2Cu (Figure 3a). The hardness of smaller specimens was much higher due to their finer microstructure with shorter secondary arm spacing, smaller interdendritic spaces and finer IQC and Θ-Al_2Cu particles (Figure 3b).

3.2. Heat Treatment

Figure 3 shows the ageing behaviour of the alloys after being heated from the as-cast state to the ageing temperatures of 300 and 400 °C. The hardness dropped immediately after the beginning of ageing in all cases. The hardness recovery started after several hours at 300 °C, and about after half an hour at 300 °C. For the most alloys, the hardness attained the highest value approximately after one week of ageing (168 h) at 300 °C and thereafter, did not change a lot. The maximum hardness was attained after 1 h of ageing at 400 °C. Thereafter, only a slow decrease of hardness was noticed. The hardness of the smaller samples (4 and 6 mm) was much higher than the 10 mm

sample. The properties did not fall below the hardness in the as-cast condition, even after the longest ageing times.

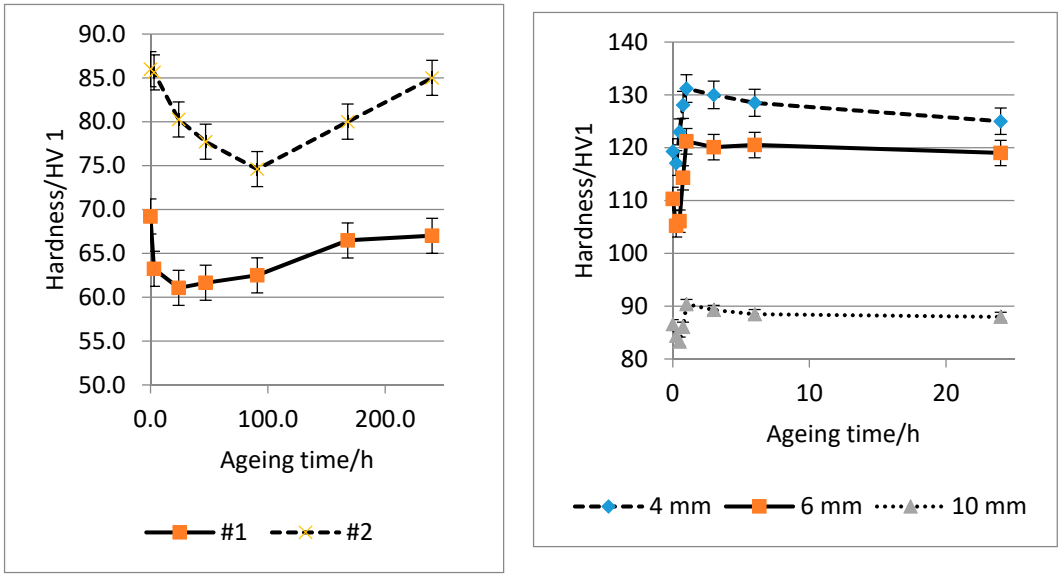

(**a**) (**b**)

Figure 3. Hardness of the alloys in the as-cast state and after heat treatment. (**a**) Hardness of different alloys aged at 300 °C (sample diameter 10 mm), (**b**) hardness of different samples of the alloy $Al_{95.4}Mn_{1.8}Cu_{1.6}Be_{1.2}$ heat-treated at 400 °C. (#1—$Al_{96.5}Mn_{0.8}Cu_{1.2}Be_{1.5}$, #2—$Al_{95.4}Mn_{1.8}Cu_{1.6}Be_{1.2}$).

Figure 4 shows the backscattered electron micrographs of some alloys aged at 300 and 400 °C. The primary and eutectic IQC particles hardly changed, while Θ-Al_2Cu became more compact. The micrographs at higher magnifications clearly showed that there were many precipitates in the α-Al matrix. Their sizes were smaller than 100 nm. The images indicate that the particles have mainly spherical shape, but it was difficult to discern more details from the SEM micrographs.

Heat treatment did not considerably change the XRD diffractograms (Figure 2). The aluminium peaks moved slightly to smaller angles because the lattice parameters of α-Al increased to 404.48 ± 0.03 pm for all alloys and samples aged at 300 and 400 °C. The supersaturation with Cu and Mn considerably decreased along with precipitation. The fraction of Θ-Al_2Cu slightly decreased, while its lattice parameters did not change. The positions and shapes of peaks in the 10 mm sample of the alloy $Al_{95.4}Mn_{1.8}Cu_{1.6}Be_{1.2}$ remain almost the same, suggesting that the structure of primary and IQC did not change. On the other hand, the peak at 15.20° became wider and moved to a higher angle (indicated by the rectangle). This is a result of precipitation of IQC in the matrix that also has a smaller lattice parameter than primary and eutectic IQC. Its value was about 0.46 [24], the same as in binary Al-Mn alloys [25]. However, the IQC precipitates had a quasilattice constant of 0.35 nm in an Al-Mn-Cu-Be-Sc-Zr alloy [19], and the same happened in this case.

For the TEM investigation, the 4 mm diameter samples of the alloy $Al_{95.4}Mn_{1.8}Cu_{1.6}Be_{1.2}$ were chosen because they had the most uniform and finest microstructure. In addition, the hardness of these samples was higher, indicating the highest values that can be achieved by heat treatment of castings.

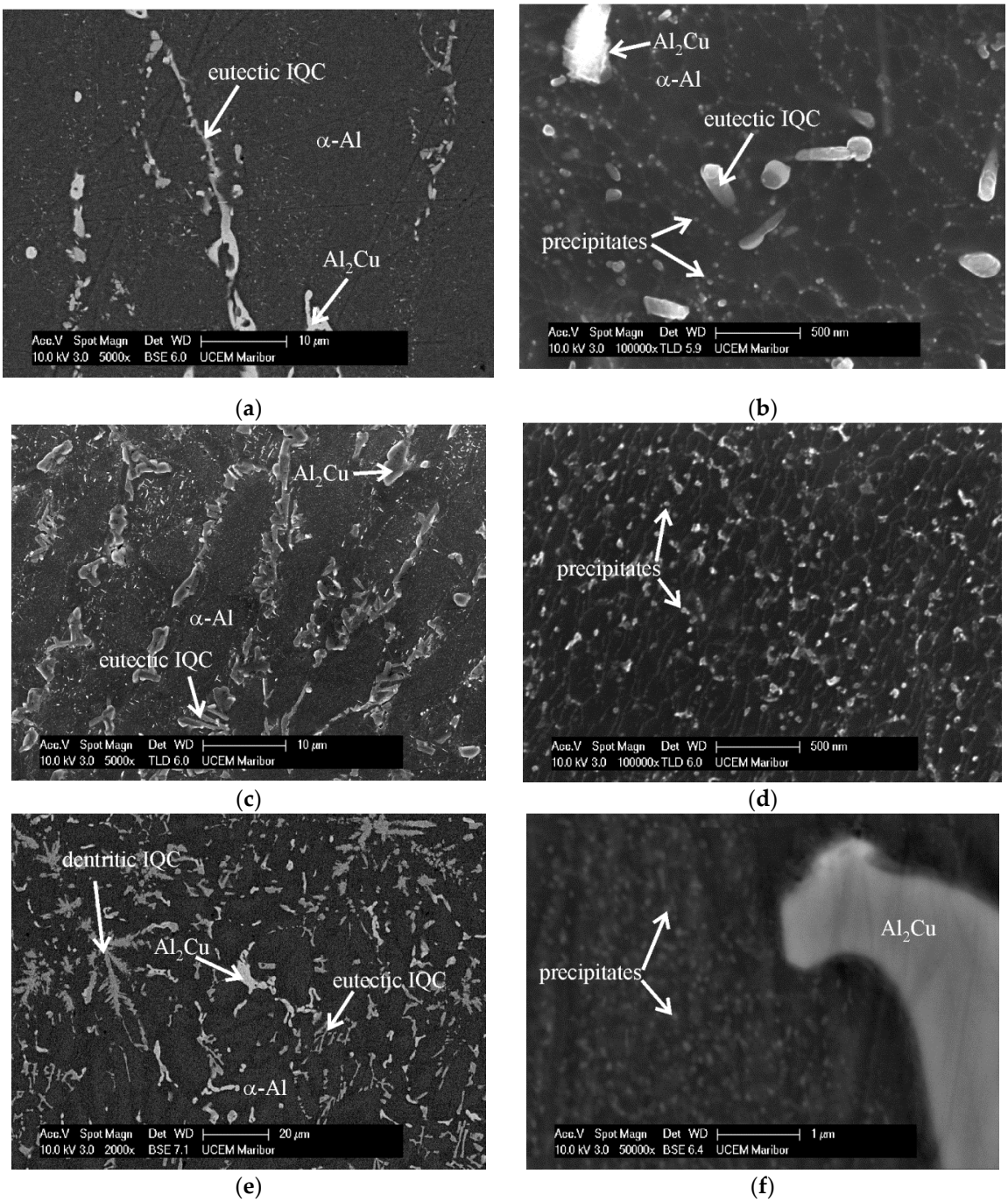

Figure 4. Backscattered electron micrographs of the alloys. (**a**,**b**) $Al_{96.5}Mn_{0.8}Cu_{1.2}Be_{1.5}$ and (**c**,**d**) $Al_{95.4}Mn_{1.8}Cu_{1.6}Be_{1.2}$ aged at 300 °C for 168 h, and (**e**,**f**) the alloy $Al_{95.4}Mn_{1.8}Cu_{1.6}Be_{1.2}$ aged at 400 °C for 1 h. The diameter of samples was 10 mm. The samples were etched using a methanol-iodine solution.

Figure 5a shows the typical microstructure of a 4 mm sample. The cell diameters are 3–5 μm, which is 2–3 times smaller than in the 10 mm samples. IQC and Θ-Al_2Cu were at the cell boundaries (Figure 5b,c). The precipitation free zone was around cell boundaries, and there was a high precipitate density within the cells. Figure 6 shows precipitates in samples aged at 300 and 400 °C. At 300 °C, a very high density of spheroidal precipitates formed that were smaller than 20 nm (16.9 ± 1.5 nm). At some places, even three precipitates were one above another within the TEM lamella, which was about 80–90 nm thick. In such cases, the distances between particle centres could be about 30 nm

(Figure 6b). The interparticle distances were up to 50 nm elsewhere. At 400 °C, slightly larger spheroidal particles were formed (26.4 ± 2.5 nm), accompanied by plate-like particles with the thickness of 15.6 ± 3.0 nm, and the length 58.4 ± 7.6 nm. The interparticle distances were larger than at 300 °C. No other precipitates (e.g., Cu-rich (Θ-Al_2Cu, θ′ or θ″), T-$Al_{20}Mn_3Cu$ or Be-rich precipitates) were identified in the microstructure.

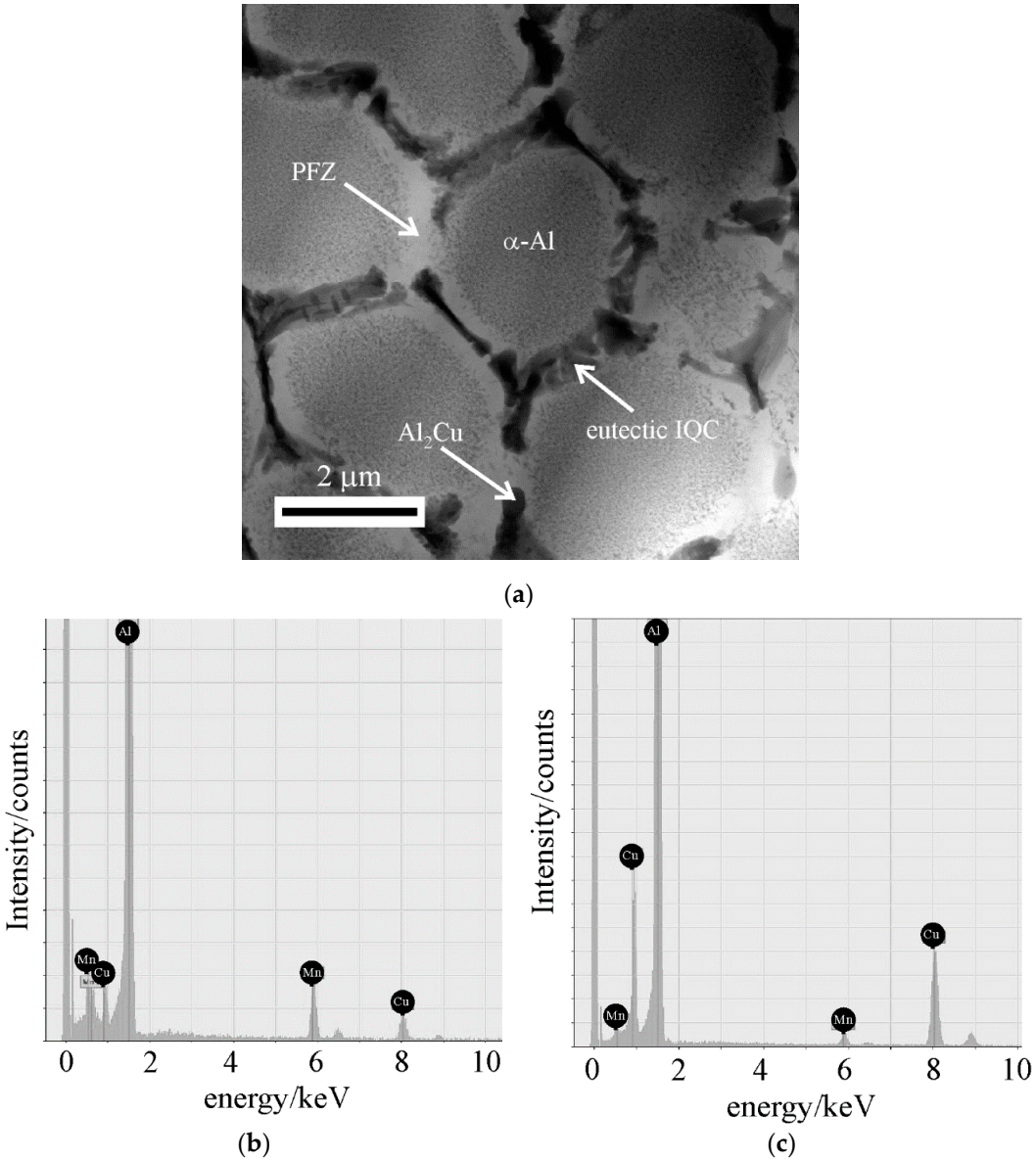

Figure 5. (**a**) Bright field transmission electron micrograph of the alloy $Al_{95.4}Mn_{1.8}Cu_{1.6}Be_{1.2}$ after ageing at 400 °C for 1 h; sample diameter 4 mm (PFZ—precipitation free zone). (**b**) EDS spectrum of the eutectic IQC and (**c**) of Θ-Al_2Cu.

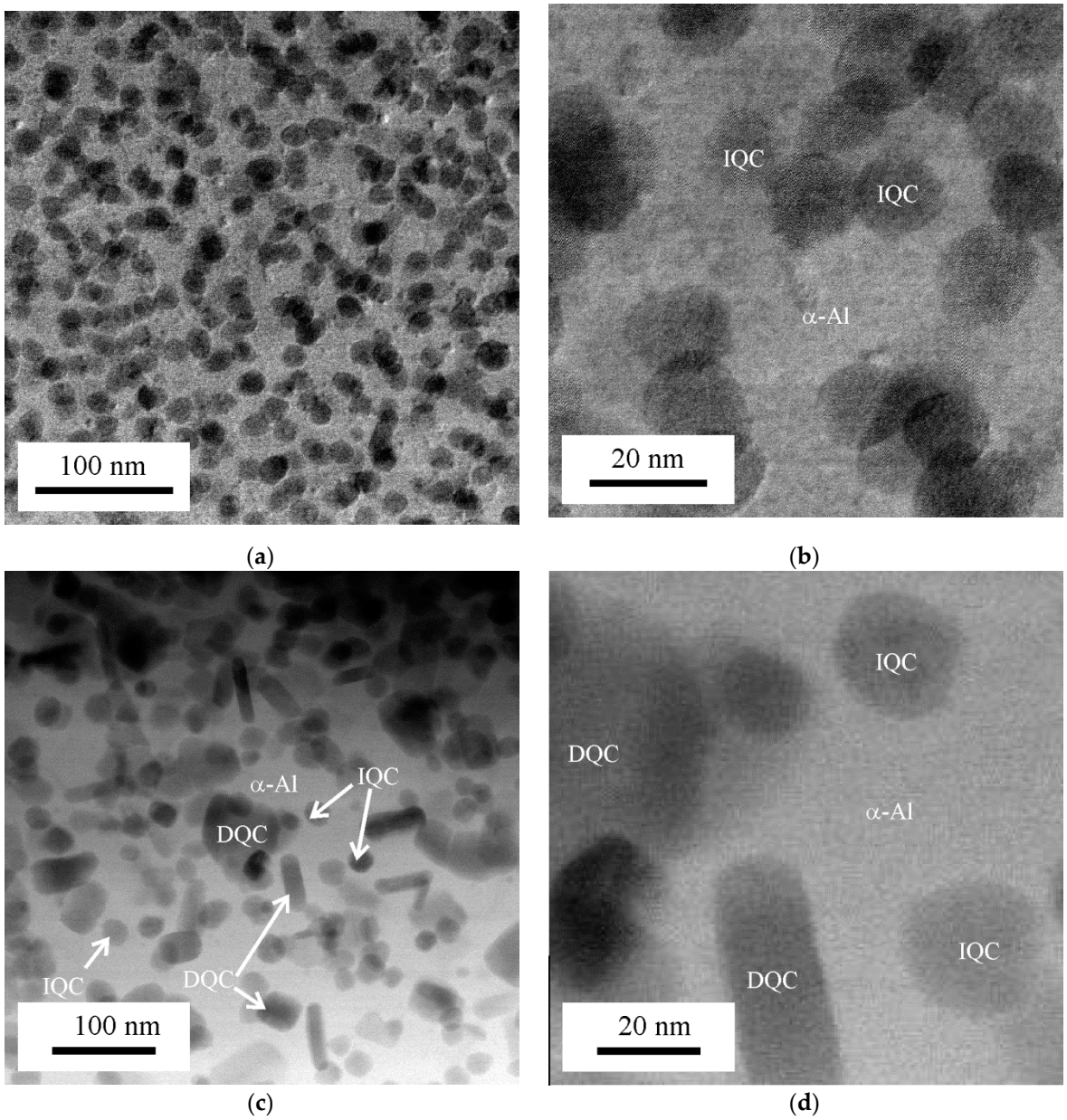

Figure 6. Bright-field TEM micrographs of the alloy $Al_{95.4}Mn_{1.8}Cu_{1.6}Be_{1.2}$ (**a**,**b**) heat-treated at 300 °C for 168 h and (**c**,**d**) heat-treated at 400 °C for 1 h (orientation close to [001]-Al). Sample diameter 4 mm. (IQC—icosahedral quasicrystal, DQC—decagonal quasicrystal).

3.3. Analysis of Icosahedral and Decagonal Quasicrystalline Precipitates

Figure 7a shows a HRTEM image of a spheroidal precipitate in α-Al. The EDS in TEM showed that it consisted of Al, Mn and some Cu (Figure 7b). EDS was not able to reveal Be. The fast-Fourier-transform (FFT) of the whole area showed the superposition of two patterns, which are shown separately in Figure 7d,e. The distances between the peaks in the directions denoted by arrows were not the same, and increased with the golden mean τ (Figure 7c,e). This clearly showed the quasicrystalline nature of the spherical precipitates; their icosahedral quasicrystalline structure was identified in detail in the previous works [16,17,19].

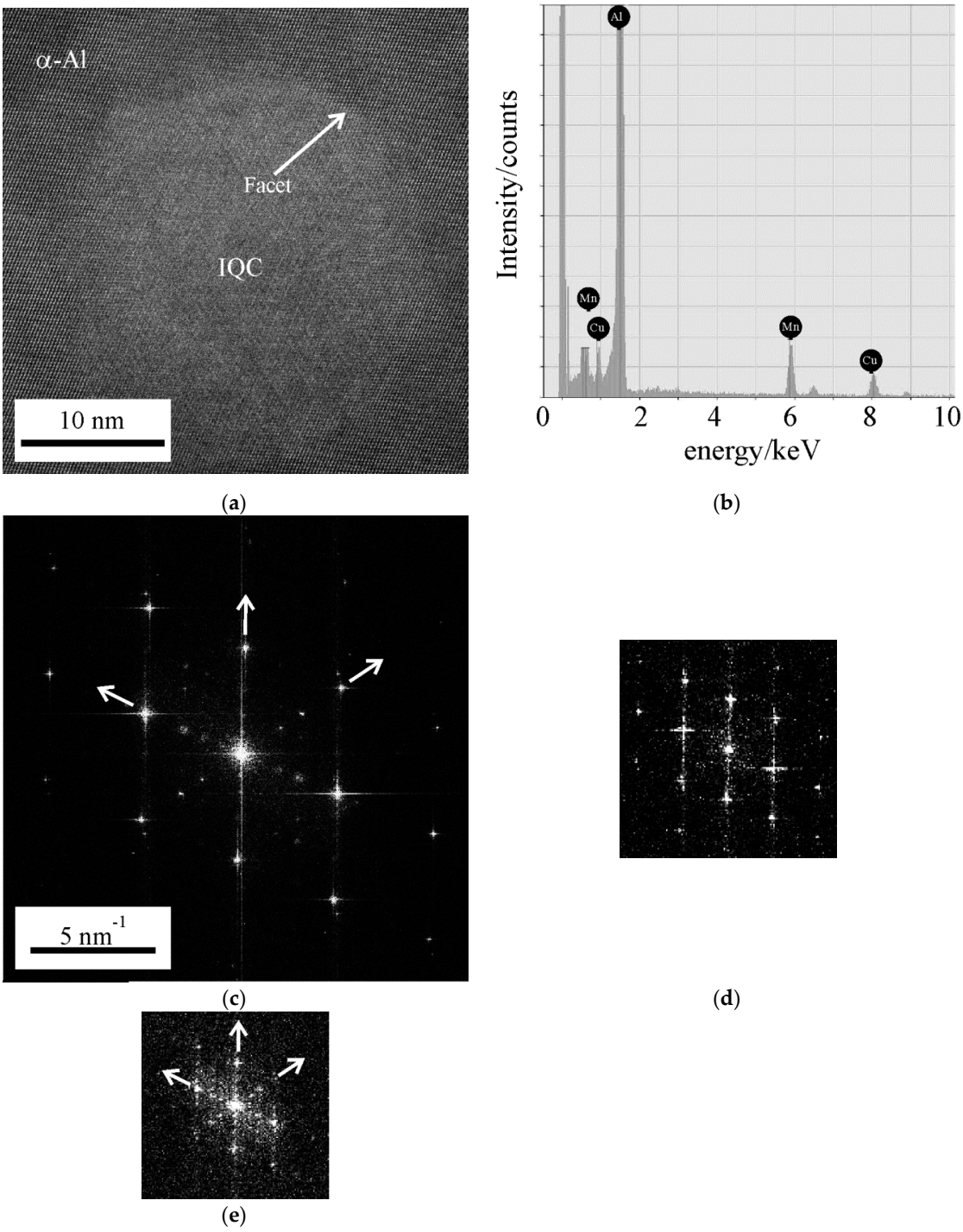

Figure 7. An icosahedral quasicrystalline (IQC) precipitate in $Al_{95.4}Mn_{1.8}Cu_{1.6}Be_{1.2}$ after ageing at 400 °C for 1 h. (**a**) A high-resolution scanning transmission electron image, (**b**) an EDS spectrum of the IQC particle, (**c**) Fast Fourier transform (FFT) of all area, (**d**) FFT of Al-rich matrix, with the zone axis [111], (**e**) FFT of the IQC particle, with the threefold zone axis $\left[01\bar{1}0\right]$.

A closer inspection showed that the threefold axis of the α-Al [111] was parallel to the threefold axis of the IQC $\left[01\bar{1}0\right]$ (indices according to Singh and Ranganathan [26]). The same orientation relationship between α-Al and IQC was found in a melt-spun Al-Mn-Si alloy [27]. A quasilattice constant of 0.35 nm was inferred, which is smaller than in the Al-Mn quasicrystal, calculated using the Elser's scheme [25]. HRTEM reveals that the IQC precipitate was not completely spherical but showed tendency to faceting. This was also found by IQC particles formed during rapid solidification [28,29].

IQC quasicrystals have predominantly shapes of pentagonal dodecahedrons, in which each facet has a shape of a regular pentagon. Due to a high symmetry of icosahedral quasicrystal, the shape appears spherical at lower magnifications.

The plate-like precipitates were identified as decagonal quasicrystalline precipitates (Figure 8a). They also consisted mainly of Al, Mn, with a small amount of Cu (Figure 8b). Their predominant habitus planes represented all three {001} planes of the α-Al. The FFTs of the HRTEM image showed the orientation relationship between DQC and FCC matrix (Figure 8c–e). For a precipitate lying on the (001) plane of the α-Al, its tenfold axis was parallel to the [010] direction of the α-Al, while its twofold axis was parallel to the [100] direction of the α-Al. The same orientation relationship was also found in the Al-Mn-Cu-Be alloys, containing Sc and Zr [19].

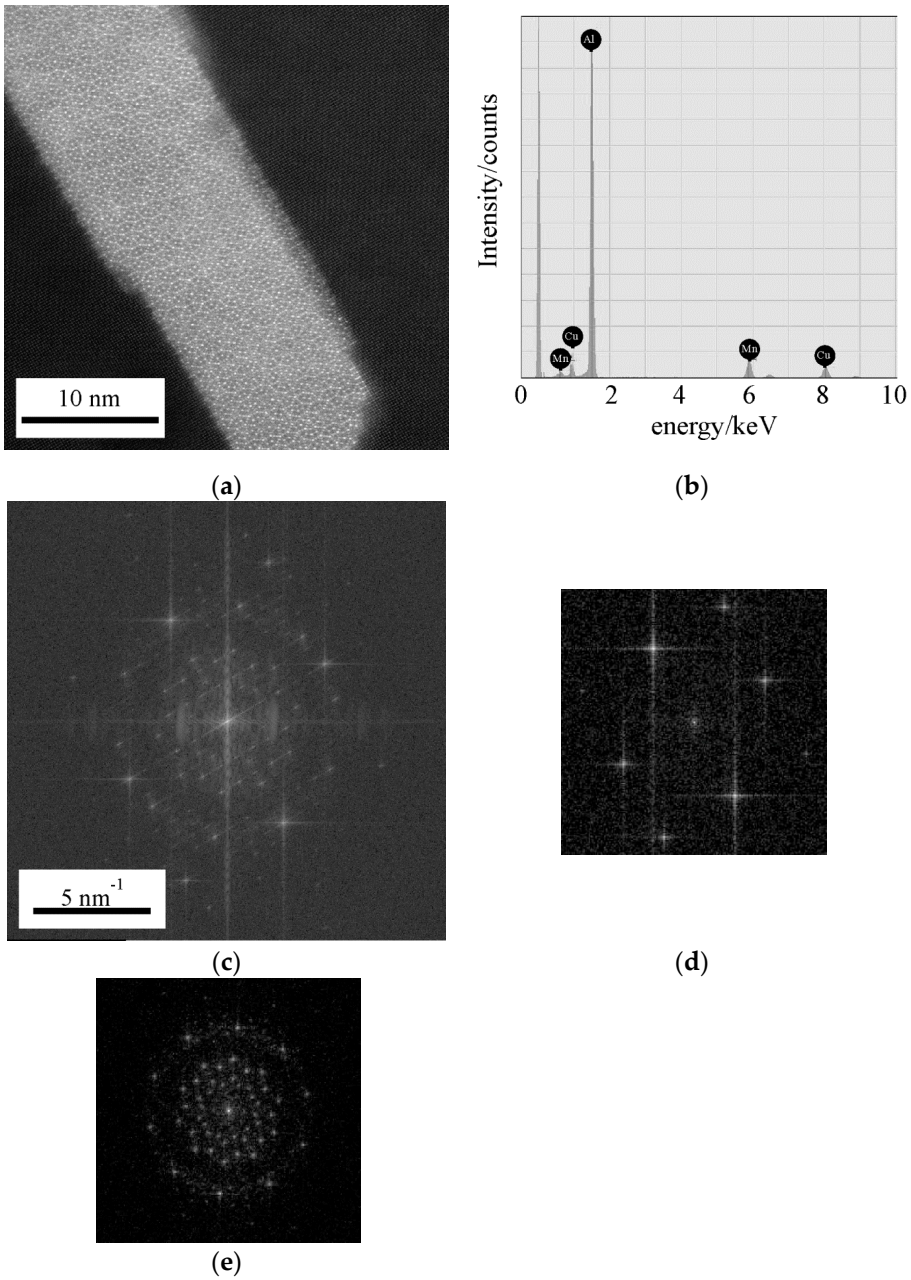

Figure 8. A decagonal quasicrystalline (DQC) precipitate in $Al_{95.4}Mn_{1.8}Cu_{1.6}Be_{1.2}$ after ageing at 400 °C for 1 h. (**a**) A high-resolution scanning transmission electron image, taken with a HAADF detector (High-angle Annular Dark Field), (**b**) an EDS spectrum of the IQC particle, (**c**) FFT of the entire area, (**d**) FFT of Al-rich matrix, with the zone axis [001], (**e**) FFT of the DQC particle along its tenfold axis.

3.4. Compression Test and Microstructures of Deformed Samples

Figure 9 shows the stress–strain diagram of the alloy $Al_{95.4}Mn_{1.8}Cu_{1.6}Be_{1.2}$ at room temperature. The yield stress σ_y is slightly above 300 MPa. At the beginning, the work hardening is very high, and the alloy attained the highest true stress σ_m = 461 MPa at true strain φ = 0.1. The softening took place up to $\varphi \approx 0.6$. The final hardening occurred until the appearance of cracks on the specimen surface at $\varphi \approx 0.8$. The barrelling started to occur at a deformation of 0.4 but was rather slight (insert in Figure 9). Thus, the value of the true stress at $\varphi \approx 0.8$ should be up to 5% lower.

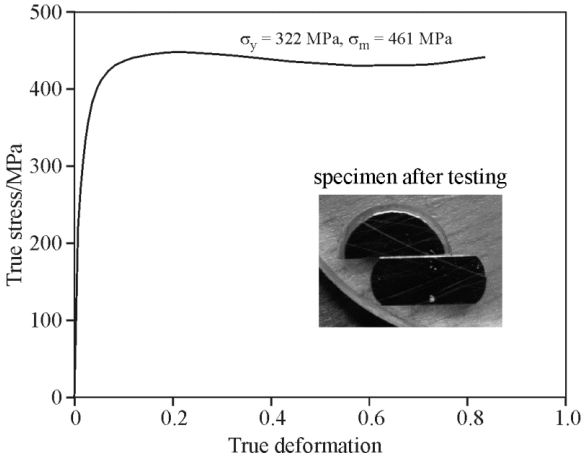

Figure 9. The compression test of the alloy $Al_{95.4}Mn_{1.8}Cu_{1.6}Be_{1.2}$ after ageing at 400 °C for 1 h, 6 mm sample. The specimen after testing is shown.

Figure 10 shows TEM micrographs after compression for φ = 0.1, which is close to the maximum on the compression curve. This deformation caused fracture of IQC and Θ-Al_2Cu at cell centres (Figure 10a). Darker regions in Figure 11b have higher dislocation density. The dislocations were almost absent in PFZ and areas with lower precipitate density (Figure 10c), but much higher in the areas with higher precipitate densities. In spite of good matching with the matrix, it is rather unlikely that dislocations could cut the particles (Figure 10d). It is more probable that the Orowan mechanism is responsible for the strengthening.

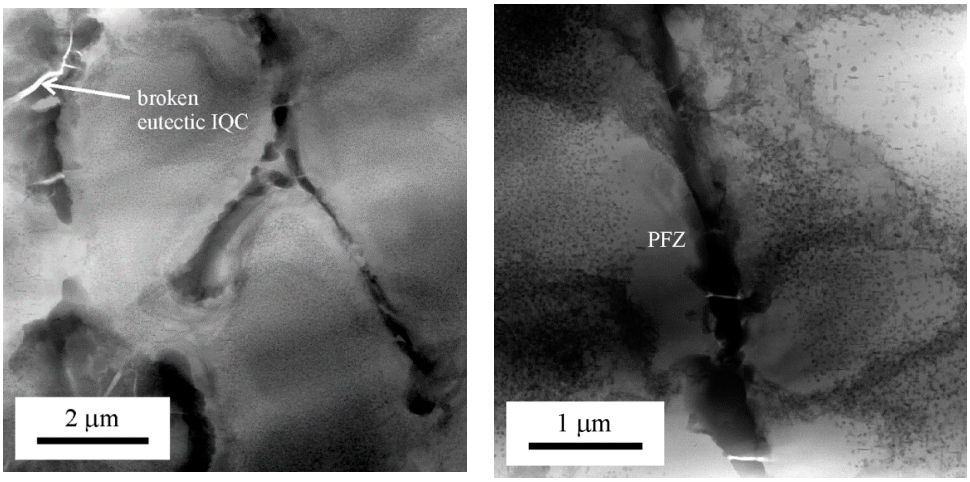

(**a**) (**b**)

Figure 10. *Cont.*

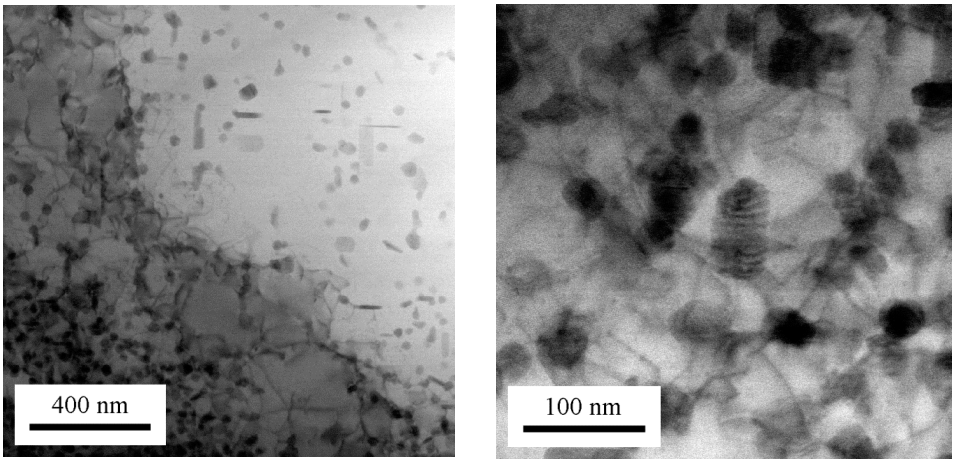

(**c**) (**d**)

Figure 10. Bright field TEM micrographs of the alloy $Al_{95.4}Mn_{1.8}Cu_{1.6}Be_{1.2}$ aged at 400 °C for 1 h and compressed with 0.09 true stress. (**a**) Deformed cells, (**b**) cell boundary with the precipitation free zone, (**c**) areas with different precipitate densities, (**d**) an area, with a higher precipitate density.

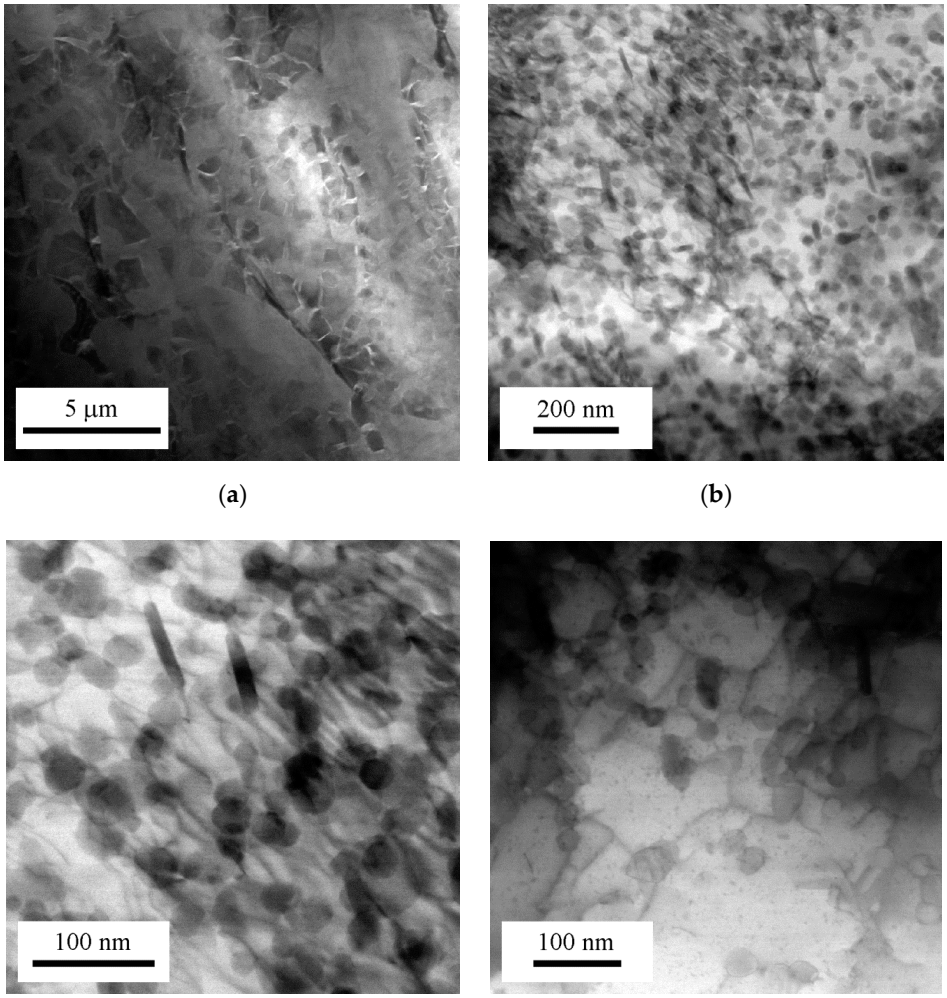

(**a**) (**b**)

(**c**) (**d**)

Figure 11. Bright field TEM micrographs of the alloy $Al_{95.4}Mn_{1.8}Cu_{1.6}Be_{1.2}$ aged at 400 °C for 1 h and compressed with 0.4 true strain. (**a**) Broken phases at a cell boundary, (**b**) an area inside a cell, (**c**) an area, with a higher precipitate density, (**d**) an area, with a lower precipitate density.

Figure 11 depicts TEM micrographs after compression for $\varphi = 0.4$. This deformation caused fragmentation of IQC and Θ-Al_2Cu formed during solidification (Figure 11a). The dislocations were more uniformly distributed (Figure 11b), however, there was still higher density of dislocations in regions with a higher precipitation density (Figure 11c,d).

4. Discussion

The supersaturation of the solid solution matrix with alloying elements and vacancies is a prerequisite for the formation of precipitates during ageing [30]. By T5 treatment, an alloy is cooled from an elevated temperature shaping process and then, artificially aged. In this investigation, casting represented the elevated shaping process and supersaturation can be achieved by sufficiently fast cooling from the liquid state, which can cause the fine microstructure besides supersaturation. The examination revealed the formation of a metastable IQC phase during solidification. The samples of all alloys with diameters from 4 to 10 mm have the same lattice parameters in the as-cast state, indicating similar supersaturation with Cu and Mn, which was close to their maximum equilibrium solubility in α-Al. This suggests the similar attainable volume fraction of precipitates in all alloys. Further increase of supersaturation can be achieved by rapid solidification, but not by typical casting processes. The Be content is essential for the formation of the quasicrystalline phase during solidification with the cooling rates obtained in the copper mould (250–600 K s^{-1}). It is incorporated in the IQC phase in rather high amounts [24,31].

The equilibrium intermetallic phases at ageing temperatures of the investigated alloys are expected to be Θ-Al_2Cu and τ_1 from the ternary Al-Mn-Cu system [32], while Be should be found in $Be_4Al(Cu,Mn)$ [24]. None of these phases appeared during ageing. The microstructure hardly changed at the ageing temperatures, indicating that only a small amount of primary phases dissolved. Thus, only the elements already present in the solid solution could contribute to the precipitation. The ageing temperature was above the solvus lines for GP zones, Θ″ and Θ′ Cu-rich precipitates [22]. There were no rod-like T-$Al_{20}Mn_3Cu_2$ that could be as well formed in Al-Mn-Cu-Be alloys at higher temperatures and in many other Al-alloys containing Cu and Mn [17,33].

The dominant phase that occurred in the studied temperature range was IQC. A high-resolution electron image (Figure 7a) showed excellent matching with α-Al, which was found also in other investigations [16,17,19]. Good matching between quasicrystalline and periodic crystals was found in many systems by Singh and Tsai [34–36], which is based on a high symmetry of IQC that can allow good correspondence between different planes of IQC and periodic crystals. Good matching also lowers the interfacial energy. In this alloy, the faceting tendency of IQC precipitates with a diameter of only 25 nm was observed. It is likely that they adopt a shape of pentagonal dodecahedron, which is surrounded by high density pentagons, further decreasing the surface energy. The spheroidal shape of IQC precipitates also implies low deformation energy by their formation. IQC precipitates have been found in many Al-alloys [14,15,37], however, their number density was rather low. It is believed that Be plays an important role by the formation of IQC precipitates. Beryllium was found at the centre of the IQC phase formed during the solidification, because it stimulates the icosahedral order in the melt [31]. It seems highly probable that Be acts in an analogous way in the solid state and initiates the formation of the quasicrystalline precipitates. Its atomic diameter (R = 111.3 pm) is about 22% less than Al. When a Be atom substitutes an Al atom at the lattice site, it can cause considerable distortion of the lattice, which may stimulate the nucleation of an IQC precipitate. After nucleation, the growth of the spheroidal IQC precipitates is limited by the diffusion of Mn, which has a much smaller diffusion coefficient than copper [38]. The growth of IQC precipitates is rather slow, since the coarsening rate of spherical precipitates is proportional to the square root of time [39].

In Al-Mn-Cu alloys, decagonal quasicrystals can form upon solidification [23,40]. The decagonal Al-Mn-Cu phase is closely related to the equilibrium phase τ_1. Thus, it is surely more thermodynamically stable than IQC. However, it is much less symmetrical. It causes more deformation during formation, thus, it appeared in a plate-like shape. Its habitus planes are (001), because they have the lowest

modulus of elasticity (62 GPa compared to 76 GPa of (111) planes). The growth of decagonal plates can take place linearly with time, so their lengthening rate is much higher than that of IQC precipitates. As a result, the appearance of DQC precipitates is a disadvantage, when considering the number density of precipitates. It would be desirable to obtain predominantly IQC precipitates. In this respect, ageing at 400 °C represents the highest viable temperature.

A lot of precipitates formed during ageing at investigated temperatures, however, the hardness remained more or less the same level as in the as-cast state. This can be contributed to the competition between the solid solution and precipitation strengthening. Nevertheless, typical aluminium alloys lose most of their strengths when heated to temperatures above 250 °C [41], but the room temperature hardness of these alloys remained at high levels after ageing for 240 h at 300 °C and 24 h at 400 °C. In order to reveal the real potential of these alloys for high temperature applications, their high temperature stability should be compared with conventional alloys at the same testing conditions.

5. Conclusions

The main conclusions of this work are:

In the investigated Al-Mn-Cu-Be alloys, the highest number density of spherical IQC precipitates, with the 15–20 nm diameters, can be obtained at 300 °C by T5 treatment.

Increasing ageing temperatures caused formation of coarser IQC precipitates and plate-like decagonal quasicrystalline precipitates.

Higher hardness was attained in the alloy possessing a higher Mn content.

The room temperature hardness of aged alloys remained more or less at the same level as in the as-cast condition.

The precipitates caused strong work hardening during initial plastic deformation up to 0.1 true strain, followed by strain softening at higher strains.

The investigated alloys showed interesting behaviour; however, further investigations are required to reveal the real potential of these experimental alloys, especially for high temperature applications.

6. Patents

The results of this investigation were very important by application of the following patent. ZUPANIČ, Franc, BONČINA, Tonica. Manufacturing of high strength and heat resistant aluminium alloys strengthened by dual precipitates = Herstellung von Hochfesten und wärmebeständigen durch dual-präzipitate verstärkten Aluminiumlegierungen = Fabrication d'alliages d'aluminium à haute résistance mécanique et thermique renforcés par des précipités doubles: European patent specification EP 3 456 853 B1, 2020-02-19. Munich: European Patent Office, 2020.

Author Contributions: Conceptualization, T.B. and F.Z.; methodology, T.B.; formal analysis, T.B.; investigation, T.B. and M.A.; writing—original draft preparation, T.B.; writing—review and editing, T.B. and M.A.; visualization, T.B. and M.A.; supervision, F.Z. All authors have read and agreed to the published version of the manuscript.

Funding: The XRD investigations were carried out at Elettra, Sincrotrone Trieste, Italy, in the framework of Proposals 20160145 and 20165196. The TEM investigations at TU Graz were enabled by the ESTEEM 3 Project, which has received funding from the European Union's HORIZON 2020 RESEARCH AND INNOVATION PROGRAMME UNDER GRANT AGREEMENT NO 823717. The authors acknowledge the financial support from the Slovenian Research Agency (research core funding No. P2-0120 and P2-0123).

Acknowledgments: We acknowledge Luisa Barba for support by XRD experiments at Elettra, Christian Gspan for S/TEM investigations, and Jaka Burja for compression tests.

Conflicts of Interest: The authors declare no conflict of interest.

References

1. Shechtman, D.; Blech, I.; Gratias, D.; Cahn, J.W. Metallic phase with long-range orientational order and no translational symmetry. *Phys. Rev. Lett.* **1984**, *53*, 1951–1953. [CrossRef]

2. Schurack, F.; Eckert, J.; Schultz, L. Synthesis and mechanical properties of cast quasicrystal-reinforced Al-alloys. *Acta Mater.* **2001**, *49*, 1351–1361. [CrossRef]
3. Huo, S.; Mais, B. Characteristics of heat resistant nanoquasicrystalline PM aluminum materials. *Met. Powder Rep.* **2017**, *72*, 45–50. [CrossRef]
4. Inoue, A.; Kimura, H. Fabrications and mechanical properties of bulk amorphous, nanocrystalline, nanoquasicrystalline alloys in aluminum-based system. *J. Light Met.* **2001**, *1*, 31–41. [CrossRef]
5. Kim, K.B.; Xu, W.; Tomut, M.; Stoica, M.; Calin, M.; Yi, S.; Lee, W.H.; Eckert, J. Formation of icosahedral phase in an Al93Fe3Cr2Ti2 bulk alloy. *J. Alloys Compd.* **2007**, *436*, L1–L4. [CrossRef]
6. Kim, S.H.; Song, G.S.; Fleury, E.; Chattopadhyay, K.; Kim, W.T.; Kim, D.H. Icosahedral quasicrystalline and hexagonal approximant phases in the Al-Mn-Be alloy system. *Philos. Mag. A Phys. Condens. Matter Struct. Defects Mech. Prop.* **2002**, *82*, 1495–1508. [CrossRef]
7. Schurack, F.; Eckert, J.; Schultz, L. Al-Mn-Ce quasicrystalline composites: Phase formation and mechanical properties. *Philos. Mag.* **2003**, *83*, 807–825. [CrossRef]
8. Boncina, T.; Markoli, B.; Zupanic, F. Characterization of cast Al86Mn3Be11 alloy. *J. Microsc.-Oxf.* **2009**, *233*, 364–371. [CrossRef] [PubMed]
9. Rouxel, B.; Ramajayam, M.; Langan, T.J.; Lamb, J.; Sanders, P.G.; Dorin, T. Effect of dislocations, Al3(Sc,Zr) distribution and ageing temperature on θ′ precipitation in Al-Cu-(Sc)-(Zr) alloys. *Materialia* **2020**, *9*, 100610. [CrossRef]
10. Babaniaris, S.; Ramajayam, M.; Jiang, L.; Langan, T.; Dorin, T. Tailored precipitation route for the effective utilisation of Sc and Zr in an Al-Mg-Si alloy. *Materialia* **2020**, *10*, 100656. [CrossRef]
11. Vončina, M.; Medved, J.; Kores, S.; Xie, P.; Schumacher, P.; Li, J. Precipitation microstructure in Al-Si-Mg-Mn alloy with Zr additions. *Mater. Charact.* **2019**, *155*, 109820. [CrossRef]
12. Mikhaylovskaya, A.V.; Mochugovskiy, A.G.; Levchenko, V.S.; Tabachkova, N.Y.; Mufalo, W.; Portnoy, V.K. Precipitation behavior of L12 Al3Zr phase in Al-Mg-Zr alloy. *Mater. Charact.* **2018**, *139*, 30–37. [CrossRef]
13. Hansen, V.; Gjønnes, J. Quasicrystals in an aluminium alloy matrix and the transformation to α-AlMnSi via intermediate stages. *Philos. Mag. A* **1996**, *73*, 1147–1158. [CrossRef]
14. Li, Y.J.; Arnberg, L. Quantitative study on the precipitation behavior of dispersoids in DC-cast AA3003 alloy during heating and homogenization. *Acta Mater.* **2003**, *51*, 3415–3428. [CrossRef]
15. Mochugovskiy, A.; Tabachkova, N.; Mikhaylovskaya, A. Annealing induced precipitation of nanoscale icosahedral quasicrystals in aluminum based alloy. *Mater. Lett.* **2019**, *247*, 200–203. [CrossRef]
16. Boncina, T.; Zupanic, F. In situ tem study of precipitation in a quasicrystal-strengthened al-alloy. *Arch. Metall. Mater.* **2017**, *62*, 5–9. [CrossRef]
17. Zupanič, F.; Wang, D.; Gspan, C.; Bončina, T. Precipitates in a quasicrystal-strengthened Al–Mn–Be–Cu alloy. *Mater. Charact.* **2015**, *106*, 93–99. [CrossRef]
18. Shen, Z.; Liu, C.; Ding, Q.; Wang, S.; Wei, X.; Chen, L.; Li, J.; Zhang, Z. The structure determination of Al20Cu2Mn3 by near atomic resolution chemical mapping. *J. Alloys Compd.* **2014**, *601*, 25–30. [CrossRef]
19. Zupanič, F.; Gspan, C.; Burja, J.; Bončina, T. Quasicrystalline and L12 precipitates in a microalloyed Al-Mn-Cu alloy. *Mater. Today Commun.* **2020**, *22*, 100809. [CrossRef]
20. Bončina, T.; Zupanič, F. Methods of Deep Etching and Particle Extracting for Controlling of Aluminium Alloys. *Mater. Today Proc.* **2019**, *10*, 248–254. [CrossRef]
21. Predel, B. Al-Mn (Aluminum-Manganese). In *Ac-Ag....Au-Zr: Supplement to Subvolume IV/5A (Landolt-Börnstein: Numerical Data and Functional Relationships in Science and Technology—New Series) (No. 4)*; Springer: Berlin/Heidelberg, Germany, 2006; ISBN 978-3540435341.
22. Predel, B. Al-Cu (Aluminum-Copper). In *Ac-Ag....Au-Zr: Supplement to Subvolume IV/5A (Landolt-Börnstein: Numerical Data and Functional Relationships in Science and Technology—New Series) (No. 4)*; Springer: Berlin/Heidelberg, Germany, 2006; ISBN 978-3540435341.
23. Stan-Glowinska, K. Formation of Quasicrystalline Phases and Their Close Approximants in Cast Al-Mn Base Alloys Modified by Transition Metals. *Crystals* **2018**, *8*. [CrossRef]
24. Rozman, N.; Medved, J.; Zupanic, F. Microstructural evolution in Al-Mn-Cu-(Be) alloys. *Philos. Mag.* **2011**, *91*, 4230–4246. [CrossRef]
25. Elser, V. Indexing problems in quasicrystal diffraction. *Phys. Rev. B* **1985**, *32*, 4892–4898. [CrossRef] [PubMed]
26. Singh, A.; Ranganathan, S. On the indexing and reciprocal space of icosahedral quasicrystal. *J. Mater. Res.* **1999**, *14*, 4182–4187. [CrossRef]

27. Fung, K.K.; Zhou, Y.Q. Direct observation of the transformation of the icosahedral phase in (Al6Mn)1−xSix, into α(AlMnSi). *Philos. Mag. B* **1986**, *54*, L27–L31. [CrossRef]
28. Boncina, T. Shapes of the icosahedral quasicrystalline phase in melt-spun ribbons. *Metalurgija* **2013**, *52*, 65–67.
29. Chattopadhyay, K.; Ravishankar, N.; Goswami, R. Shapes of quasicrystals. *Prog. Cryst. Growth Charact. Mater.* **1997**, *34*, 237–249. [CrossRef]
30. Andersen, S.J.; Marioara, C.D.; Friis, J.; Wenner, S.; Holmestad, R. Precipitates in aluminium alloys. *Adv. Phys. X* **2018**, *3*, 1479984. [CrossRef]
31. Zupanic, F.; Markoli, B.; Naglic, I.; Weingartner, T.; Meden, A.; Boncina, T. Phases in the Al-Corner of the Al-Mn-Be System. *Microsc. Microanal.* **2013**, *19*, 1308–1316. [CrossRef]
32. Lukas, H.L. Al-Cu-Mn (Aluminium-Copper-Manganese). In *Light Metal Systems. Part 2*; Effenberg, G., Ilyenko, S., Eds.; Springer: Berlin/Heidelberg, Germany, 2005; Volume 11A2. Available online: https://materials.springer.com/lb/docs/sm_lbs_978-3-540-31687-9_5 (accessed on 10 July 2020). [CrossRef]
33. Belov, N.A.; Alabin, A.N.; Matveeva, I.A. Optimization of phase composition of Al-Cu-Mn-Zr-Sc alloys for rolled products without requirement for solution treatment and quenching. *J. Alloys Compd.* **2014**, *583*, 206–213. [CrossRef]
34. Singh, A.; Somekawa, H.; Tsai, A.P. Interfaces made by tin with icosahedral phase matrix. *Scr. Mater.* **2008**, *59*, 699–702. [CrossRef]
35. Singh, A.; Somekawa, H.; Matsushita, Y.; Tsai, A.P. Solidification of tin on quasicrystalline surfaces. *Philos. Mag.* **2012**, *92*, 1106–1128. [CrossRef]
36. Singh, A.; Tsai, A.P.; Nakamura, M.; Watanabe, M.; Kato, A. Nanoprecipitates of icosahedral phase in quasicrystal-strengthened Mg-Zn-Y alloys. *Philos. Mag. Lett.* **2003**, *83*, 543–551. [CrossRef]
37. Mikhaylovskaya, A.V.; Kishchik, A.A.; Kotov, A.D.; Rofman, O.V.; Tabachkova, N.Y. Precipitation behavior and high strain rate superplasticity in a novel fine-grained aluminum based alloy. *Mater. Sci. Eng. A* **2019**, *760*, 37–46. [CrossRef]
38. Du, Y.; Chang, Y.A.; Huang, B.Y.; Gong, W.P.; Jin, Z.P.; Xu, H.H.; Yuan, Z.H.; Liu, Y.; He, Y.H.; Xie, F.Y. Diffusion coefficients of some solutes in fcc and liquid Al: Critical evaluation and correlation. *Mater. Sci. Eng. A Struct. Mater. Prop. Microstruct. Process.* **2003**, *363*, 140–151. [CrossRef]
39. Christian, J.W. CHAPTER 16—Precipitation from Supersaturated Solid Solution. In *The Theory of Transformations in Metals and Alloys*; Christian, J.W., Ed.; Pergamon: Oxford, UK, 2002; pp. 718–796.
40. Štrekelj, N.; Naglič, I.; Klančnik, G.; Nagode, A.; Markoli, B. Microstructural changes in quasicrystalline Al–Mn–Be–Cu alloy after various heat treatments. *Int. J. Mater. Res.* **2015**, *106*, 342–351. [CrossRef]
41. Kaufman, J.G. *Properties of Aluminium Alloys—Tensile, Creep and Fatigue Data at High and Low Temperatures*; ASM International: Metals Park, OH, USA, 1999.